Journal of Computers Vol. 37 No. 4, August 2026, pp. 311-327
https://doi.org/10.63367/19911599202608370401 8

Research on Adaptive Sliding Mode Control Parameter Optimization for Permanent Magnet Synchronous Motor Based on Reinforcement Learning and Simulation Analysis

Xiao-Long Tian[1,2], Peng Zhang[1], Hai-Tao Li[1,2*], Tao Wang[1],
Sheng-Wu Kong[1], Jia Cui[1], and Qing-Chuan Liu[1]

[1] Hebei Mechanical and Electrical Polytechnic,
Xingtai City 054000, Hebei Province, China

[2] Xingtai Technology Innovation Centre for Intelligent Welding and Cutting Engineering,
Xingtai City 054000, Hebei Province, China

tianxiaolong@hbjd.edu.cn, zhangpeng@hbjd.edu.cn, lht3236@163.com,
wangtao@hbjd.edu.cn, hbjdksw@163.com, cuijia@hbjd.edu.cn, hbjdlqc@126.com

Received 10 July 2026; Revised 31 July 2026; Accepted 24 August 2026

Abstract. The permanent magnet synchronous motor (PMSM) has been extensively applied in high-performance drive systems because of its high efficiency, compact construction, and superior dynamic performance. However, the design and implementation of traditional sliding mode control (SMC) systems have to be very dependent on the parameter selection, which could possibly lead to the increase of chattering and decreased adaptability under different operating conditions. In order to solve these problems, an SMC controller parameter optimization method based on reinforcement learning (RL) is put forward in this paper. The proposed RL-based SMC controller parameter optimization algorithm integrates RL into the sliding mode control process, and the adaptive adjustment of the control parameters can be realized through feedback from the performance of the controlled system. Specifically, the system states consist of the speed tracking error, the current error, and the sliding surface characteristic; the optimization goal contains the tracking accuracy, the convergence performance, and the chattering suppression. Simulation experiments on MATLAB/Simulink are performed to validate the effectiveness of the proposed method. The results show that, compared with the traditional SMC, the RL-based adaptive SMC control scheme can achieve good dynamic performance, less steady-state error, chattering reduction, and disturbance rejection.

Keywords: sliding mode observer, sliding mode control, sensorless control, phase-locked loop, permanent magnet synchronous motor

1 Introduction

Permanent magnet synchronous motors (PMSMs) are widely used in industrial servo applications due to their high energy conversion efficiency, reliable operation performance, and relatively compact mechanical structure [1]. Typical PMSM drives employ a cascaded control architecture, including outer-loop position control, middle-loop speed control, and inner-loop current control, and use space vector pulse width modulation (SVPWM) to generate inverter switching signals [2]. In traditional closed-loop systems, mechanical sensors measure the rotor's angular position and rotational speed to provide feedback to the controller. While this approach can provide direct status information, the additional sensing devices increase hardware costs and system complexity. In addition, factors such as temperature changes, humidity, mechanical vibration, and electromagnetic interference can also reduce its measurement accuracy and operational stability. These limitations reduce the robustness of the drive system and limit the application of position and speed sensors in harsh industrial environments [3]. PMSMs are multivariable, strongly coupled nonlinear systems and are also affected by external factors such as mechanical vibration and transmission backlash [4]. Therefore, intelligent control methods are often employed to address PMSM nonlinearity and external disturbances, including fuzzy control, model reference adaptive control, neural network control, and sliding mode control. Fuzzy control avoids the influence of parameter variations and external load changes through predefined fuzzy rules, but the establishment of these rules relies

* Corresponding Author

heavily on designer experience [5]. Model reference adaptive control is suitable for systems whose accurate mathematical models are difficult to obtain and can automatically adjust online according to parameter or load changes; however, the design of adaptive control laws is difficult. Neural network control requires a large amount of training data. Sliding mode control, on the other hand, features strong anti-interference capability, insensitivity to model parameter variations, nonlinear control characteristics, and high system stability, and has therefore been widely applied [6]. Though sliding mode control has very good robustness in regard to uncertainty and disturbance of models, the design of control performances heavily relies on the design of sliding mode parameters. Poor setting of parameters will cause problems such as excessive chattering, slow convergence rate, and low tracking accuracy. The traditional way of designing the parameters only relies on engineering experience or offline optimization, thus limiting the adaptive ability of the controller under different operational conditions. The recently emerging field of reinforcement learning (RL) has received considerable attention for intelligent control systems since it is able to learn strategies from the environment. Based on observation and feedback reward signals, reinforcement learning enables controllers to update their control parameters without knowing priori about the system dynamics. In this respect, reinforcement learning in combination with sliding mode control could be considered as an efficient method to realize adaptive parameter optimization. The paper considers the application of a parameter optimization strategy based on reinforcement learning to automatically tune the sliding mode control parameters. Considering the strong robustness and adaptability of sliding mode control for PMSM nonlinear systems, a PLL sliding mode observer is designed in this study. A saturation function approaching law is employed to improve observation stability and ensure the accuracy of back electromotive force estimation. To address the issues associated with traditional position sensors, such as high costs, susceptibility to environmental interference, and insufficient robustness under complex operating conditions, a control method based on a Phase-Locked Loop (PLL) and a Sliding Mode Observer (SMO) is proposed. First, the paper reviews the current state of PMSM control systems and the application of SMOs in rotor position and speed estimation, highlighting the urgent need for improvements in chattering suppression, phase lag reduction, and handling parameter uncertainties. On this basis, PLL technology is utilized to filter the estimated BEMF, thereby accurately obtaining rotor position and speed information. The simulation results demonstrate that the method maintains excellent speed tracking performance and position estimation accuracy under conditions of load disturbances and parameter variations. exhibiting robust stability and offering an effective solution for intelligent sensorless the PMSM control.

2 Literature Review

Researchers are investigating how to control permanent magnet synchronous motors (PMSMs) through the use of sliding mode current observers for stable control [7]. Sliding mode current observers exhibit robustness, accurate measurement, and the ability to resist disturbance. Previous work by Shao et al. provides insight into the use of sliding mode observers (SMOs) for electric machines and shows that they can be used effectively for robust state estimation, despite system uncertainties [8]. Recent research continues to focus on PMSMs using SMOs to improve both robustness and accuracy. For example, Chen et al. modified an existing current observer by employing a PI regulator instead of traditional sliding mode switching functions to effectively address issues associated with chattering and phase delay, while still providing the benefits of robust performance [9]. Recent research has also attempted to improve the dynamic response and robustness of PMSMs by developing more sophisticated reaching law algorithms. Liu et al. proposed an exponential reaching law and the use of arcsine saturation functions, which improved both chattering and observer error performance [10]; Zhong et al. provided a means of improving upon this through the design of an improved sliding mode observer (ISMO) that is integrated with a disturbance observer [11]. Exponential input functions and an integral sliding surface were incorporated to improve both anti-disturbance performance and dynamic robustness. Observers designed using fuzzy logic and intelligent algorithms also evolved through research. Huang et al. provided an improved fuzzy super-twisted sliding mode observer as another means of reducing chattering and improving estimation accuracy [12]; this indicates a trend toward adaptive and intelligent observers. The literature also shows that sliding mode observers have been integrated with fault-tolerant and sensorless control methods. For instance, Hart et al. employed a long short-term memory (LSTM) network in conjunction with a neural network-based fault-tolerant control strategy to provide a way to predict current states and identify faults [13]; this enhances reliability during periods of sensor failure. Wang et al. also conducted research into developing disturbance

observers and predictive model control strategies [14], both of these offered sensorless operation based upon sliding mode observers, thus exhibiting robustness with respect to parameter mismatches and load disturbances. As noted above, there has been a shift toward more sophisticated and adaptive robust designs of SMOs. These advancements are critical for providing PMSMs with stable, accurate, and resistance to disturbances; such systems are important in applications requiring high performance. Basing current state-of-the-art PMSM control systems on SMOs using innovative approaches, including developing novel reaching law methodologies, innovative filtering techniques, and intelligent algorithms, will help address the challenges associated with "chattering," phase delay, and, to a reasonable level, uncertainties in the control systems.

3 Methodology

This section describes a PM servo drive developed using a mathematical model and a sensorless estimation process, assuming that the stator EMF and rotor air gap magnetic field have sinusoidal waveforms, with hysteresis and eddy current losses being ignored. The theoretical foundation for developing the sliding mode observer is provided by deriving equations for PMSM voltage and current in a stationary $\alpha - \beta$ coordinate system. The sliding mode observer uses stator current as an observable variable and defines the difference between estimated and actual currents as an error that serves as the switching surface for the observer. The current estimation error dynamic is established by formulating the sliding mode current observer and subtracting the estimated PMSM current equation from the actual PMSM current equation to determine the current estimation error. There is also a limit to the maximum gain of the sliding mode controller based on the sliding mode controller's reachability, existence, and stability. However, if the magnitude of the gain is too large, then it is likely to result in chattering at high frequencies, thereby increasing the estimation error, thus the need for a rational methodology for gain selection arises. To reduce chattering, the saturating function replaces the normal changing from sign function in the PMSM controlled system. The saturating function allows the PMSM controlled system to function in a narrow band about the switching surface and, as a result, reduces high frequency oscillations and increases the current estimator performance. Under ideal conditions, there will be no current estimation error, and the back EMF can be estimated using the estimated current to actual current error. The rotor speed and/or position can then be determined using the arctangent of the estimated back EMF. Since back EMF may be affected by chattering as well, the current estimation error will need to be filtered from each other through the use of a phase-locked loop (PLL) and a proportional-integral (PI) control loop. The PI control loop will be used to provide an estimation of rotor speed that can then be integrated to yield a rotor position estimate. Ultimately, through the use of the PLL and the PI control loop, the estimated rotor position and estimated rotor speed will agree with the actual values and thus provide better PMSM sensorless control stability and accuracy.

3.1 Mathematical Model of Permanent Magnet Synchronous Motor

It is assumed that the stator armature winding induces sinusoidal electromotive force, the rotor air-gap magnetic field distribution is sinusoidal, and hysteresis and core eddy current losses are neglected [15]. Under the stationary $\alpha - \beta$ coordinate system, the voltage equation of the PMSM is given by Equation (1).

$$\begin{pmatrix} u_\alpha \\ u_\beta \end{pmatrix} = R_S \begin{pmatrix} i_\alpha \\ i_\beta \end{pmatrix} + \begin{pmatrix} L_s & 0 \\ 0 & L_s \end{pmatrix} \begin{pmatrix} \frac{di_\alpha}{dt} \\ \frac{di_\beta}{dt} \end{pmatrix} + \begin{pmatrix} e_\alpha \\ e_\beta \end{pmatrix} \tag{1}$$

According to Equation (1), the PMSM current equation under the stationary $\alpha - \beta$ coordinate system can be obtained as Equation (2):

$$\frac{di_s}{dt} = -\frac{R_s}{L_s} i_s + \frac{1}{L_s} u_s - \frac{1}{L_s} e_s \tag{2}$$

The aforementioned mathematical model describes the fundamental relationships among stator voltage, stator current [16]. Operating in the $\alpha - \beta$ coordinate system allows for the direct characterization of the motor's electrical dynamics without requiring additional coordinate transformations based on rotor position, thereby simplifying the design of sensorless estimation algorithms. The voltage equations indicate that variations in stator current depend on the applied voltage, stator resistance, inductance parameters, and the induced back-EMF. Since information regarding rotor position is embedded within the back-EMF term, accurate estimation of the back-EMF is crucial for obtaining rotor position and speed data in sensorless control systems in Table 1.

Table 1. Parameters and assumptions used in PMSM mathematical modeling

Parameter	Description	Assumption/Value
Motor type	Permanent magnet synchronous motor	Surface-mounted PMSM
Coordinate system	Reference frame for modeling	Stationary coordinate system
Stator EMF waveform	Distribution of induced voltage	Sinusoidal waveform
Rotor air-gap magnetic field	Magnetic field distribution	Sinusoidal waveform
Hysteresis loss	Magnetic hysteresis effect	Ignored
Eddy-current loss	Core eddy-current effect	Ignored
Stator resistance	Electrical resistance parameter	Considered in the voltage model
Stator inductance	Electrical dynamic parameter	Considered in the current model
Back EMF	Rotor position information source	Estimated by observer
Observable variable	Sliding mode observer input	Stator current

3.2 Sliding Mode Observer

The three-phase stator current is used as the control variable, and the difference between the measured current and the reconstructed current defines the switching surface of the sliding mode observer [17]. Under the sliding mode mechanism, the reconstructed current gradually converges to its measured value. For practical applications, the observer's switching function employs a constant-gain discontinuous switching law. According to Equation (2), the PMSM sliding mode current observer can be established as Equation (3):

$$\frac{d\hat{i}_s}{dt} = -\frac{R_s}{L_s}\hat{i}_s + \frac{1}{L_s}u_s - \frac{1}{L_s}k\,\mathrm{sgn}(i_s - i_s) \tag{3}$$

The current error equation can be obtained as:

$$\frac{d\tilde{i}_s}{dt} = -\frac{R_s}{L_s}\tilde{i}_s + \frac{1}{L_s}e_s - \frac{1}{L_s}k\,\mathrm{sgn}(\hat{i}_s - i_s) \tag{4}$$

Where the current error is defined accordingly. According to the reachability, existence, and stability conditions of the sliding mode observer: The above equation can be rewritten in the stationary $\alpha - \beta$ coordinate system as:

$$\tilde{i}_\alpha{}^T[-\frac{R_s}{L_s}\tilde{i}_\alpha - \frac{1}{L_s}e_\alpha - \frac{1}{L_s}k\,\mathrm{sgn}(\hat{i}_\alpha - i_\alpha)] \le 0 \tag{5}$$

$$\tilde{i}_\beta{}^T[-\frac{R_s}{L_s}\tilde{i}_\beta - \frac{1}{L_s}e_\beta - \frac{1}{L_s}k\,\mathrm{sgn}(\hat{i}_\beta - i_\beta)] \le 0 \tag{6}$$

The sliding mode gain satisfies:

$$\tilde{i}_{\alpha}^{T}[-\frac{1}{L_s}e_{\alpha}-\frac{1}{L_s}k\,\mathrm{sgn}(\hat{i}_{\alpha}-i_{\alpha})]\le 0 \tag{7}$$

$$\tilde{i}_{\beta}^{T}[-\frac{1}{L_s}e_{\beta}-\frac{1}{L_s}k\,\mathrm{sgn}(\hat{i}_{\beta}-i_{\beta})]\le 0 \tag{8}$$

However, the sliding mode gain should not be excessively large, otherwise the chattering phenomenon will increase and unnecessary estimation errors will be generated [18]. Therefore, the sliding mode gain can be selected according to:

$$k=\lambda\psi_f\,|\psi_r| \tag{9}$$

In the design of the sliding mode observer, the switching control sign function is defined as:

$$z=k\,sign(x) \tag{10}$$

In practical applications, the sliding mode control system operates in a small region around the switching surface, resulting in high-frequency motion near the switching surface. Therefore, the saturation switching function is introduced:

$$z=\begin{bmatrix}Z_{\alpha}\\Z_{\beta}\end{bmatrix}=k\times sat(S_{\alpha,\beta})=\begin{cases}k & S_{\alpha,\beta}>\Delta\\ ks/\Delta, & -\Delta\le s(x)\le\Delta\\ -k & S_{\alpha,\beta}<\Delta\end{cases} \tag{11}$$

The chattering of the sliding mode observer during operation can be suppressed. In this paper, the saturation function is used to replace the sign function as the switching control function, thereby improving the performance of current sliding mode control [19]. Consequently, the observer maintains stable estimation performance even under conditions of load variation or model uncertainty. However, the traditional sign switching function suffers from an inherent “chattering” drawback. The high-frequency switching behavior generated by the sign function introduces unwanted oscillations into the estimated back EMF, thereby compromising the accuracy of rotor position and speed estimation [20]. In practical PMSM drive systems, excessive chattering exacerbates current fluctuations, reduces control efficiency, and can even induce mechanical vibrations. Therefore, an appropriate switching strategy is required to strike a balance between rapid convergence and estimation smoothness. Unlike the discontinuous sign function, the saturation function creates a boundary layer around the sliding-mode surface, allowing the system state to approach the surface smoothly. Within this boundary region, the switching amplitude is reduced, effectively suppressing high-frequency oscillations while maintaining sufficient robustness against disturbances. The thickness of the boundary layer dictates the trade-off between estimation accuracy and chattering suppression: a thinner boundary layer improves estimation accuracy but may increase oscillations. Whereas a thicker boundary layer ensures smoother operation but may reduce convergence accuracy. Thus, the parameters of the saturation function must be carefully selected based on the dynamic characteristics of the PMSM system. The sliding-mode gain is another critical parameter influencing observer performance. A sufficiently high gain ensures that the estimation error rapidly reaches the sliding-mode surface and enhances disturbance rejection capabilities; however, an excessively high gain increases switching frequency and intensifies chattering effects. Therefore, the selection of the gain must satisfy the stability conditions of the sliding-mode observer while avoiding unnecessary high-frequency oscillations. By optimizing the relationship between the sliding mode gain and the saturation function, the observer achieves both rapid convergence and stable estimation. However, due to switching characteristics and measurement noise, chattering components may persist in the estimated EMF signal; consequently, additional filtering strategies are required before extracting the rotor information in Table 2.

Table 2. Comparison between conventional sign-function SMO and proposed saturation-function SMO

Item	Conventional SMO	Proposed saturation-function SMO
Switching function	Sign function	Saturation function
Switching characteristic	Discontinuous switching	Smooth boundary-layer switching
Chattering phenomenon	Severe high-frequency oscillation	Effectively suppressed
Estimation error	Increased due to oscillation	Reduced estimation error
Dynamic response	Fast convergence but unstable oscillation	Fast convergence with improved stability
Robustness to disturbances	Sensitivity to parameter variations	Strong disturbance rejection capability
Back EMF estimation	Contains high-frequency noise components	Improved EMF reconstruction accuracy
Rotor position estimation	Possible phase error	Higher tracking accuracy
Control performance	Reduced current quality	Improved sensorless PMSM performance

In traditional sliding mode control, controller parameter settings depend on system characteristics and are carried out empirically. However, due to changing operating conditions, fixed parameters do not ensure optimal operation of the control system, especially in the presence of disturbances. To address this problem, in this work, a reinforcement learning-based approach to adaptive tuning of parameters is proposed. The reinforcement learning algorithm interacts with the control process and changes parameters of the sliding mode controller based on system states. As a state vector for interaction with the agent, key information about the control process is selected, which consists of such factors as speed tracking error, current tracking error, and sliding surface. These components provide information about the dynamics and stability of the control process of the PMSM system. Based on the current state, adaptive actions for parameter adjustment are generated in order to adjust the sliding mode gain. For evaluation of the control response, a set of criteria for reward computation is chosen, which include several control goals such as speed tracking accuracy, sliding surface convergence, and chattering reduction.

3.3 Acquisition of Rotor Position and Speed Information

Under ideal sliding mode control conditions, the system motion remains on the sliding surface:

$$\tilde{i}_s = \frac{d\tilde{i}}{dt} = 0 \tag{12}$$

The observed back electromotive force can be obtained:

$$\hat{e}_s = ksat(\hat{i}_s - i_s) = ksat(\tilde{i}_s) \tag{13}$$

The above equation can be rewritten in the stationary α-β coordinate system as:

$$\hat{e}_\alpha = -\hat{\omega}_r \psi_f \sin\theta_r = ksat(\tilde{i}_\alpha) \tag{14}$$

$$\hat{e}_\beta = -\hat{\omega}_r \psi_f \sin\theta_r = ksat(\tilde{i}_\beta) \tag{15}$$

Based on the above equations, the estimated rotor position and rotor speed can be obtained using the arctangent function:

$$\hat{\theta} = -\arctan(\frac{\hat{e}_\alpha}{\hat{e}_\beta}) \tag{16}$$

$$\hat{\omega}_r = \frac{\sqrt{e_\alpha{}^2 + e_\beta{}^2}}{\psi_f} \tag{17}$$

As a result, errors arise when estimating rotor position and speed using the arctangent function, which affects control accuracy. Therefore, the phase-locked loop (PLL) technology is introduced to suppress the high-frequency chattering of sliding mode control, reduce the chattering components in the estimated back electromotive force.

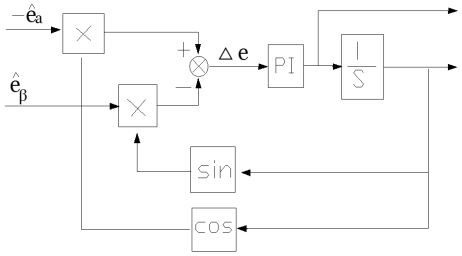

Fig. 1. The PLL block diagram

According to Fig. 1:

$$\begin{aligned}\Delta e &= -\hat{e}_\alpha \cos\hat{\theta}_{re} - -e_\beta \sin\theta_{re} \\ &= k\sin\theta^*_{re}\cos\hat{\theta}_{re} - k\cos\theta^*_{re}\sin\theta_{re} \\ &= k\sin(\theta^*_{re} - \hat{\theta}_{re})\end{aligned} \tag{18}$$

When the angle error satisfies the required condition, the equation can be written as:

$$\Delta e = k\sin(\theta^*_{re} - \hat{\theta}_{re}) \approx k\Delta\theta_{re} \tag{19}$$

Fig. 1 illustrates the rotor position and speed estimation structure based on a phase-locked loop (PLL) used in a sensorless control system. The estimated back-electromotive force (EMF) signal, obtained from a sliding-mode observer, first undergoes coordinate transformation [21]. The estimated speed signal is integrated to obtain the rotor position angle, which is then fed back to the sine and cosine calculation units, forming a closed-loop tracking structure [22]. Through continuous error correction, the estimated rotor position gradually converges to the actual rotor position, and the system ultimately achieves a stable synchronous state. Compared to direct calculation methods, the PLL structure effectively suppresses high-frequency oscillations caused by sliding-mode control. The PI controller improves dynamic response capabilities, while the feedback loop enhances tracking accuracy under varying speed and load conditions.

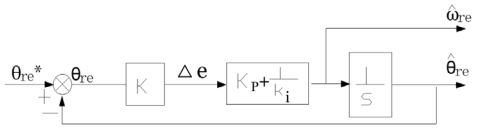

Fig. 2. The equivalent block diagram of the PLL system

Fig. 2 shows the equivalent PLL tracking algorithm corresponding to Fig. 1. As shown in Fig. 2, the rotor position error is processed through a PI controller to estimate rotor speed, and the estimated speed is integrated to obtain the rotor position. Through PLL technology, the estimated rotor position and speed can closely track the actual rotor position and speed. Fig. 2 illustrates the equivalent phase-locked loop (PLL) tracking structure

used for rotor position estimation. Designed as a closed-loop position tracking system, the PLL aims to eliminate estimation errors caused by high-frequency oscillations in the sliding-mode observer and to enhance the accuracy of rotor position and speed estimation [23]. The PLL inputs consist of a reference rotor position signal and an estimated rotor position signal derived from the observer. These two signals are compared via a subtraction unit to generate a position tracking error. This error represents the difference between the estimated and actual rotor positions and serves as the primary control variable for the PLL system [24]. First, the position error signal is processed by a proportional adjustment unit to improve the dynamic response of the tracking system. The signal is then fed into a proportional-integral (PI) controller, which further reduces steady-state error and enhances the stability of the estimation process. The controller output is the estimated rotor speed. The speed estimate is integrated to obtain the updated rotor position information, which is then fed back to the input to form a closed-loop correction structure. During operation, the phase-locked loop (PLL) continuously compares the estimated position with the reference position and adjusts the estimated speed and position through feedback. When the system reaches a locked state, the position error approaches zero, indicating that the estimated rotor position can accurately track the actual position. The combination of proportional control, integral regulation, and feedback compensation enables PLLs to achieve both fast dynamic response and high steady-state accuracy. Compared with the direct position calculation method, the proposed PLL tracking structure has better noise suppression capability and stronger robustness to parameter changes and external disturbances.

4 Reinforcement Learning-Based Optimization and Simulation Analysis

Fig. 3 illustrates the dual closed-loop SVPWM control architecture implemented on a TMS320F2812 DSP with a PLL-based current sliding-mode observer. The observer provides the estimated motor speed for feedback. The deviation between the reference and estimated speeds is then processed by a PI regulator in the outer speed loop to improve tracking performance.

$$e_w = \hat{w}_e^* - w_e \tag{20}$$

$$i^*_q = k_{pw} e_w + k_{iw} \int e_w dt \tag{21}$$

Where e_w represents the speed error, $\hat{w}_e^*$ is the reference speed, $\hat{w}_e$ is the estimated rotor speed, and i^*_q is the reference q-axis current generated by the speed controller. The q-axis current error is reduced through the PI current inner-loop controller.

$$T_e = \frac{3}{2} p \psi_f i_q \tag{22}$$

Where T_e is the electromagnetic torque, p represents the number of pole pairs, represents the permanent magnet flux linkage, and i_q is the q-axis current. The d-axis reference current is set to zero and compared with the feedback current. A PID controller is adopted in the d-axis current loop to maintain zero d-axis current. The outputs of the d-axis and q-axis current loops are transformed back into stationary two-phase currents through inverse rotational transformation and then converted into voltage signals. Space vector pulse width modulation (SVPWM) is used to realize stable motor control. The proposed dual-loop SVPWM control system integrates the advantages of sensorless rotor position estimation, vector control, and high-performance current regulation, offering an effective solution for the stable operation of permanent magnet synchronous motor (PMSM) drive systems [25]. The control system is implemented on a TMS320F2812 DSP platform, which provides real-time signal processing capabilities for motor state estimation and control execution. In this control framework, the rotor speed estimated by the PLL-based sliding mode observer serves as the feedback signal for the speed loop. Compared to traditional sensor-based control methods, sensorless speed feedback eliminates reliance on mechanical position sensors and enhances system reliability under harsh operating conditions, such as vibration, temperature fluctuations, and electromagnetic interference [26].

$$u_d^* = K_{pd} e_d + K_{id} \int e_d dt \tag{23}$$

$$u_q^* = K_{pq} e_q + K_{iq} \int e_q dt \tag{24}$$

This structure improves the motor's dynamic response and mitigates the effects of parameter coupling. The resulting current components are compared with reference values, and current errors are compensated by proportional-integral (PI) regulators [27]. By calculating the required voltage vectors, the SVPWM controller generates corresponding switching signals for the inverter, enabling it to provide smooth and precise voltage excitation to the PMSM. SVPWM offers higher DC voltage utilization, lower harmonic distortion, and superior torque control performance. Consequently, it is well-suited for high-performance Permanent Magnet Synchronous Motor (PMSM) drive systems that require precise speed regulation and rapid dynamic response. Furthermore, the sliding-mode observer utilizes measured stator current and motor voltage data to continuously estimate rotor position and speed. The estimated rotor position is fed back to the coordinate transformation module, ensuring precise synchronization between the control reference frame and the motor's actual magnetic field orientation. Combining sliding-mode observation with a Phase-Locked Loop filter effectively reduces estimation errors caused by model uncertainties and high-frequency switching interference.

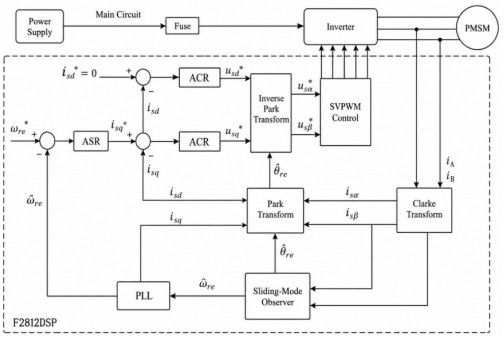

Fig. 3. The control system diagram

The system shown in Fig. 3 is simulated in Simulink. The motor parameters are in Table 3.

Table 3. Simulation parameters of the PMSM sensorless control system

Parameter	Value
Motor type	Surface-mounted PMSM
Stator resistance	3.5 Ω
Permanent magnet flux linkage	0.077 Wb
Moment of inertia	0.0008 kg·m²
Damping coefficient	0
DC bus voltage	311 V
PWM switching frequency	10 kHz
Sliding mode observer gain	Optimized value
PLL proportional gain	Tuned parameter
PLL integral gain	Tuned parameter

In order to analyze the efficacy of the designed reinforcement learning-based adaptive sliding mode controller, a qualitative analysis has been conducted comparing the classical sliding mode control system approach and the designed RL-based system, which is shown in Table 4. Dynamic response, steady-state response, chattering rejection ability, and disturbance rejection ability have been considered in the comparison process.

Table 4. Performance comparison between conventional SMO-SMC and RL-based adaptive SMC

Method	Rise time	Steady error	Chattering	Disturbance rejection
Traditional SMC	Higher	Large	Strong	Medium
RL-SMC	Lower	Small	Reduced	Strong

The reference speed is preset. The initial load torque is set at the initial moment, and the load torque changes at a specified time instant. MATLAB simulations are carried out for the estimated rotor position and speed, estimation errors, and induced electromotive force. The simulation results are shown in Fig. 4–Fig. 8.

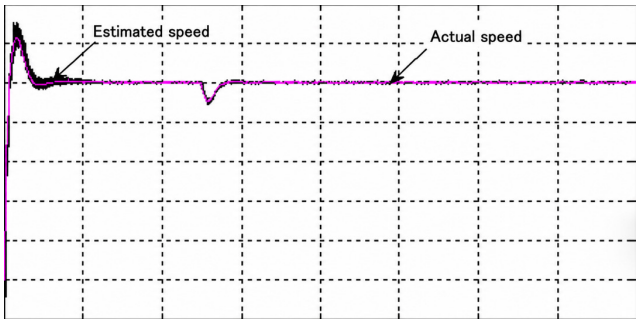

Fig. 4. The change curve between the estimated speed and the actual value

Fig. 4 outlines the comparisons carried out between the estimated speed and the actual speed of the adaptive wheel-based mobile robot through the motion process. At the beginning of the motion process, there is a transient response due to three factors: the start-up of the motors, the effect that inertia has on the robot as it accelerates to its velocity, and how quickly the control input is established. A slight overshoot occurs at motor startup, but the observer output rapidly converges to the measured value once the transient response subsides. Under steady-state conditions, the two curves exhibit close agreement, demonstrating the accuracy of the proposed method in identifying the robot's real-time motion state. Only minor oscillations are observed around the equilibrium point, indicating stable tracking performance and negligible estimation error. The middle portion of the speed response curve illustrates a localized disturbance to the speed, as the actual speed decreases for a short time. The source of this disturbance could be due to variances in the terrain, variations in the load, the nature of the track, and ground interaction, or instantaneous resistance experienced during motion, among others. Following a short-lived disturbance to speed, the system returns rapidly to the steady state; furthermore, the estimated speed continues to follow that of the actual speed with little delay. Therefore, it is concluded that the motion system of the robot has good disturbance rejection and the speed observer/estimation algorithm has good dynamic tracking performance. Overall, the close correlation between the estimated speed and the actual speed indicates that the proposed method of motion estimation and control of the robot is effective. Additionally, the results demonstrate that the adaptive wheel/track mechanism is capable of generating output at a stable speed while providing sufficient feedback from the estimation model for closed-loop control while the robot is in continuous motion. The close alignment between the estimated and actual speeds validates the effectiveness of the proposed PLL-based sliding mode observer in providing reliable feedback for closed-loop control [28]. During the initial acceleration phase, the observer undergoes a brief adjustment period due to sudden changes in electromagnetic torque and the initial discrepancy between estimated and actual motor states; however, the rapid convergence of the estimated speed demonstrates the observer's excellent dynamic response, enabling it to quickly establish accurate rotor motion data. During steady-state operation, the estimated and actual speed curves almost perfectly overlap, indicating that the observer maintains high estimation accuracy under normal operating conditions. The minimal steady-state error demonstrates that the incorporated PLL effectively filters out the high-frequency oscillations inherent in sliding mode observers, thereby enhancing the stability of the speed estimation. Under external disturbances, the motor speed only deviates from the command value briefly before quickly returning to the desired trajectory. This transient response demonstrates that the proposed controller can effectively suppress fluctuations caused by

disturbances and maintain reliable speed regulation. The shorter recovery time also indicates that the system is highly robust to sudden load changes and other operational uncertainties. Furthermore, no significant sustained oscillations or steady-state shifts were observed after the disturbance disappeared, confirming the stability of the overall control structure.

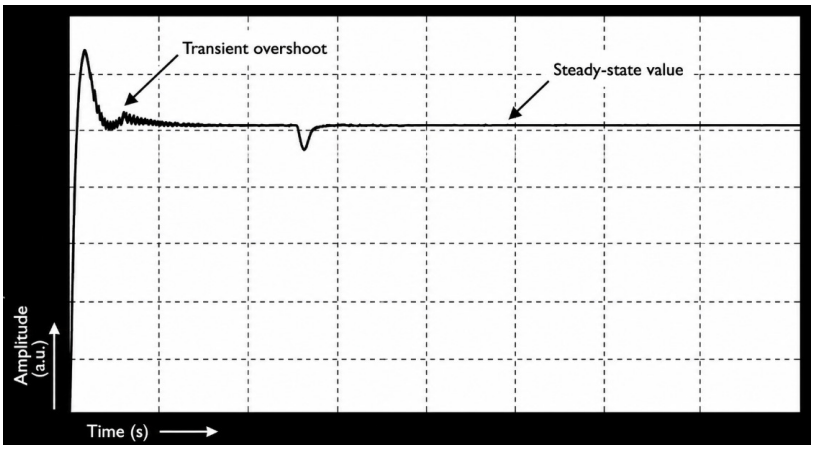

Fig. 5. The variation curve of speed estimation error

The dynamic response of an adaptive wheel-track mobile robot system subject to transient excitation is shown in Fig. 5. The horizontal axis represents time, while the vertical axis represents the normalized response amplitude in an arbitrary unit of measure. In the first part of the response, the amplitude goes up rapidly and has significant transient overshoot. The main cause for this is the sudden application of drive input; the inertial effect of the wheel-track mechanism; and, rapid adjustment of the actuator or control system. After the overshoot from the transient, the response amplitude decreases rapidly and approaches its steady-state value. The oscillations are attenuated, indicating that there is enough damping in the system and that it is dynamically stable. Other than a small local fluctuation during the response, the amplitude quickly returns to steady state, indicating that the system can suppress transient disturbances effectively. The response curve shows that in the steady-state condition, the curve remains at a nearly constant reference level with only small fluctuations about that level. This indicates that the optimization process has provided the adaptive wheel-track mechanism with stable dynamic characteristics during continuous use. The small amount of steady-state variation also indicates adequate stiffness within the structured mechanism and smooth enough control responses. In summary, the response curve shows that the system recovers rapidly from transient excitation and maintains stable output after short adjustment periods. Therefore, an optimized wheel-track mechanism is appropriate for mobile robot applications that require frequent acceleration, mode transformations, or suppression of terrain-induced disturbances. The transient response characteristics shown in Fig. 5 further demonstrate the excellent dynamic stability and disturbance rejection capabilities of the proposed adaptive wheeled-tracked hybrid mobile robot system. The initial overshoot observed at the start of the response is typical behavior for a closed-loop electromechanical system upon activation; this phenomenon stems primarily from the sudden application of control inputs, the acceleration of drive motors, and the inertia of the mechanical structure. Despite the distinct peak in the initial phase, the response rapidly decays and converges to a steady-state region, indicating that the control system possesses sufficient damping characteristics and rapid error compensation capabilities. Following the initial transient phase, the response curve maintains a relatively stable amplitude with only minor fluctuations. This low level of steady-state fluctuation indicates that the optimized mechanism possesses good structural rigidity and that the control strategy effectively maintains stable operation during continuous movement. The absence of sustained oscillation demonstrates that the system avoids excessive vibration and dynamic instability, critical factors affecting the operational reliability of mobile robots in complex environments [29].

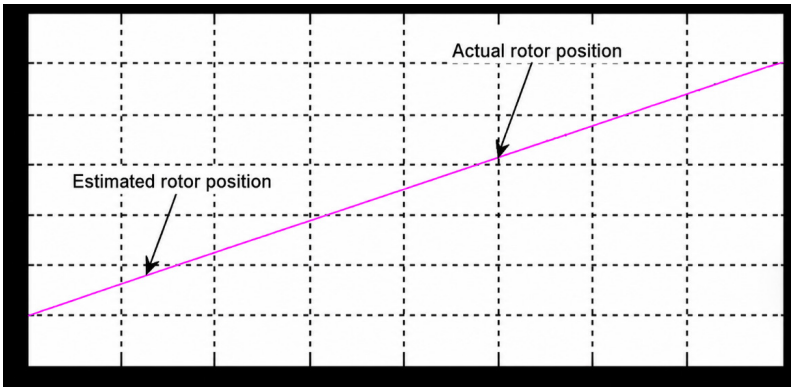

Fig. 6. The curve of the estimated value of rotor position and the actual value

Comparison of actual rotor position vs estimated rotor position throughout the driving motor's continuous rotation is shown in Fig. 6. From the graph, you can see that rotor position increases nearly linearly over time, which indicates that the motor runs at an approximately constant angular velocity during this phase. The estimated rotor position shows good correlation to the actual rotor position throughout the entire response time. The two traces essentially lie on top of each other, and there is no noticeable phase difference, divergence, or oscillatory error. This indicates the proposed rotor position estimation method is able to track real-time changes in rotor position accurately. Differences between speed response curves and rotor position curves are due to the fact that rotor position is an integrated state variable and therefore is more susceptible to estimation drift. A small speed estimation error left unchecked for a long period of time can lead to a substantial position error. However, over the entire duration of time represented in this figure, the estimated rotor position tracks consistently with the actual rotor position, confirming that the estimation algorithm has good long-term stability and does not accumulate significant errors. The nearly linear trajectory of rotor position also indicates that the motor's output is smooth during steady-state conditions. Accurate estimation of rotor position, which is directly related to track or wheel motion, allows for reliable feedback for closed-loop speed control, trajectory tracking, and control for the transformation from wheel to track mode. These findings confirm the accuracy and practical applicability of the proposed rotor-position estimation technique, thereby supporting reliable motion control of the adaptive wheel-track mobile robot. As illustrated in Fig. 6, the PLL-based sliding-mode observer maintains close agreement between the reconstructed and measured rotor-position trajectories throughout the operating period. This consistency indicates that the observer can effectively recover rotor-state information without requiring mechanical position sensors, while preserving the precision and stability needed for real-time control. The absence of significant oscillations, phase lag, or cumulative deviation confirms the estimation method's excellent tracking capability and long-term stability. During the initial phase of operation, a slight transient deviation exists between the estimated and actual rotor positions. This phenomenon primarily stems from mismatches in the observer's initial conditions, the sudden onset of electromagnetic excitation, and the adjustment process of the closed-loop estimation system [30]. However, as the sliding mode observer converges, this deviation rapidly diminishes, and the estimated rotor position gradually synchronizes with the actual position. This rapid convergence indicates that the designed observer possesses favorable dynamic response characteristics, enabling effective compensation for initial estimation errors. During steady-state operation, both curves exhibit an almost identical linear growth trend, corresponding to the constant rotational speed of the permanent magnet synchronous motor (PMSM) [31].

The time-domain amplitude response for the adaptive wheel–track system of the mobile robot under transient excitation results in Fig. 7. The horizontal axis indicates time, while the vertical axis indicates the response amplitude normalized in arbitrary units. At the start of the response, the amplitude reached a relatively high level, indicating that there was an observable transient impact associated with the system at this moment; this could be due to the motor starting, sudden mechanical load, inertial effects of the wheel–track mechanism, or quick establishment of the control input. After the initial peak response, the amplitude decreased quickly with time. The response curve shows a typical decay/attenuation process over time; thus, it can be inferred that the system has adequate capability to damp out transients and/or dynamic errors through its damping capability. The rapid decay of amplitude shows that the optimized mechanism will not cause the mobile robot's motion to foster large

sustained oscillations after an excitation event. Therefore, this enhances the mobile robot's ability to achieve motion stability. In the steady state of the response, the amplitude is low and nearly constant over time; to a small degree, there are fluctuations about the steady-state amplitude. Therefore, the system continues to operate in a stable dynamic state through its operational life. This also indicates that the optimized wheel–track mechanism has sufficient structural stiffness and that the control system is providing satisfactory residual vibration tracking error suppression capabilities. In the middle part of the response curve, there is a short, small disturbance where the amplitude quickly drops and then returns to the original steady-state value. This could be due to an instantaneous change in terrain resistance, fluctuations in how the track-ground surface is contacting, changes in load, or a short-duration adjustment made by the control system. Regardless, the period of the disturbance was brief. So the system was able to recover quickly from the disturbance without the generation of sustained oscillations or divergence. Thus, this demonstrated the ability of the adaptive wheel–track to reject disturbances as well as recover dynamically. In conclusion, the overall response from this curve demonstrates that the adaptive wheel–track mechanism can quickly attenuate initial transient responses and demonstrate good long-term steady amplitude after stabilization. This verified that the optimized mechanism exhibits dynamic stability, which supports the use of the adaptive wheel-track mobile robot to operate effectively in the presence of changing terrains and intermittently applied forces.

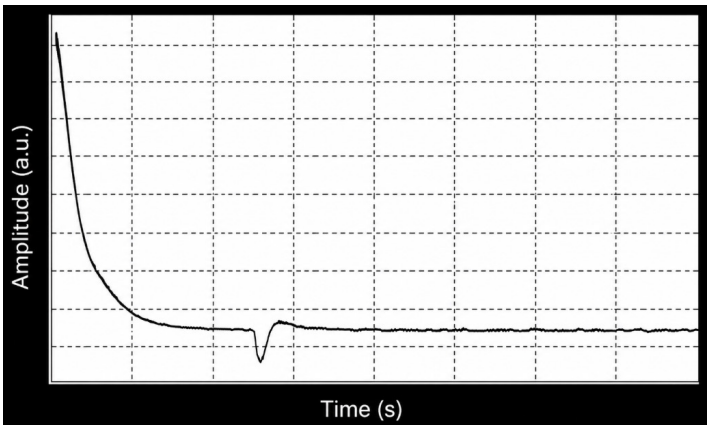

Fig. 7. The variation curve of rotor position estimation error

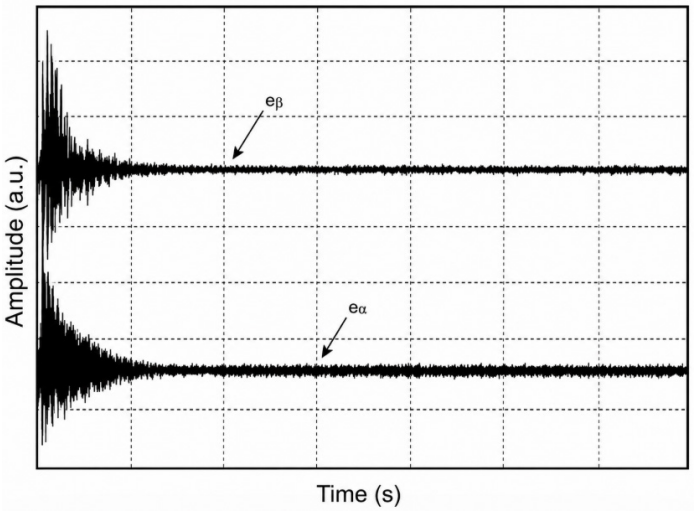

Fig. 8. The variation curves of induced electromotive force

Fig. 8 shows the time-domain response signals of e in the stationary α-β coordinate system, with time plotted on the x-axis and the normalized magnitude of the e signal on the y-axis. For all error signal components, we see significant amounts of oscillation at an early time due to reasons including (1) that the control input used is continuous, (2) that the e signal experiences a transient response while the motor is powered, (3) that there is an initial mismatch of the e signal state to the estimated state of the dynamic motor system at power-up, and (4) that the convergence rate of the observer/estimator for each motor is rapid. At time equals 0, the e signal contains high-frequency, two-dimensional transient oscillations, indicating that the overall system undergoes an extended transient adjustment period from the time the motor/locomotion control system is first energized. However, as time progresses, the amount of oscillation in the e signal decreases, indicating that the proposed control/estimator method exhibits rapid convergence characteristics. After the transient adjustment period, the e signals converge toward steady-state values; therefore, it also indicates that an observer performing estimation can continuously provide stable estimation performance after convergence without generating divergent oscillations or accumulating estimation error over time. Although both e signals exhibit similar convergence characteristics, the respective steady-state values of both indicate that each signal approximates a different near-constant level. Differences in the near-constant level may exist due to the characteristics of the respective axes of the stationary α-β coordinate systems, differences in the respective initial conditions of each e signal, differences in the uncertainties related to the model parameters, or depending upon asymmetrical dynamic characteristics associated with the respective motor-driving systems. Regardless of potential reasons for the observed difference in the near-constant level, both error signal component values exhibit stable performance following the transient adjustment period, further verifying the robustness of the control estimator methodology. The stable response curve analysis of e indicates that the adaptive wheel-track mobile robot, at all times, can rapidly reduce the initial estimation error and continue to produce low-amplitude steady-state oscillations. Therefore, the control estimator methodology is a viable approach to achieving estimation of the adaptive wheel-track mobile robot's motion state and to help achieve stable locomotion of a motor-driven adaptive wheel-track mobile robot after continuing to operate.

To test the effectiveness of the reinforcement learning based adaptive sliding mode control, the simulations are performed to compare between the standard fixed parameter sliding mode control and the optimized sliding mode controller. The objective of this experiment is to analyze the performance of the reinforcement learning to improve the adaptability of the sliding mode controller. In the optimization process, the reinforcement learning based controller learns about the system states and adjusts the parameter of the sliding mode controller based on the reward from the feedback. The system states include speed tracking error, current error and sliding surface properties. The optimization criteria include tracking performance, convergence performance and chattering reduction. The illustration of the adaptive adjustment process of the sliding mode gain is given in Fig. 9. It can be seen that the sliding mode gain is adjusted based on the dynamic response of the system, while for the standard sliding mode controller the parameter is always fixed. Specifically, the fixed-parameter controller maintains a constant sliding mode gain of 50 throughout the simulation. In contrast, reinforcement learning optimizes the controller with a lower initial gain, close to 35, and then gradually increases the gain based on the changing situation. Within the first 2 seconds, the gain rapidly increases to nearly 46, reflecting the adjustment during the initial transient phase. Between 2 and 5 seconds, the rate of increase in gain tends to level off, indicating that the controller is optimizing its response as the system behavior changes. Subsequently, the gain continued to increase and approached the fixed reference value of 50 at approximately 7 to 8 seconds, after which it remained essentially unchanged until the simulation ended. This adaptive trajectory demonstrates that reinforcement learning algorithms can identify appropriate gain values at different stages of operation, rather than applying uniform parameters throughout the control process. A relatively small initial gain helps limit excessive switching activity and reduce chattering, while a gradual increase in gain can enhance the robustness of the control and support convergence when stronger corrective measures are needed. Overall, the results show that reinforcement learning provides a practical mechanism for dynamically adjusting sliding mode control parameters based on system feedback and operational requirements.

In order to examine the dynamic response ability, the RL-SMC algorithm is compared with the conventional sliding mode control scheme with constant parameters. From Fig. 10, it can be seen that both the two schemes are capable of realizing the speed tracking, but the former exhibits better performance in dynamic response.

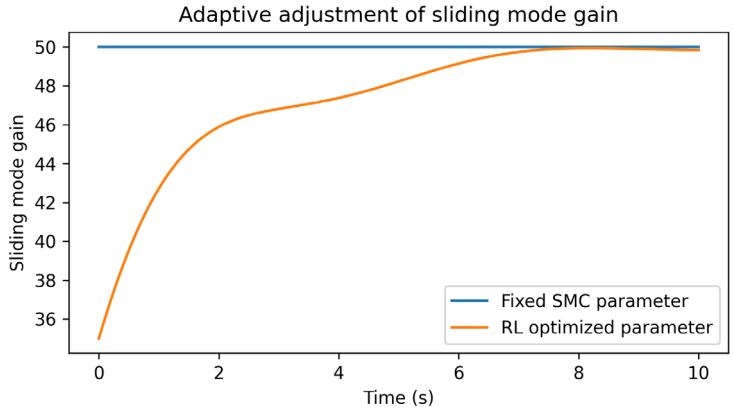

Fig. 9. Reinforcement learning-based adaptive gain tuning for sliding mode control

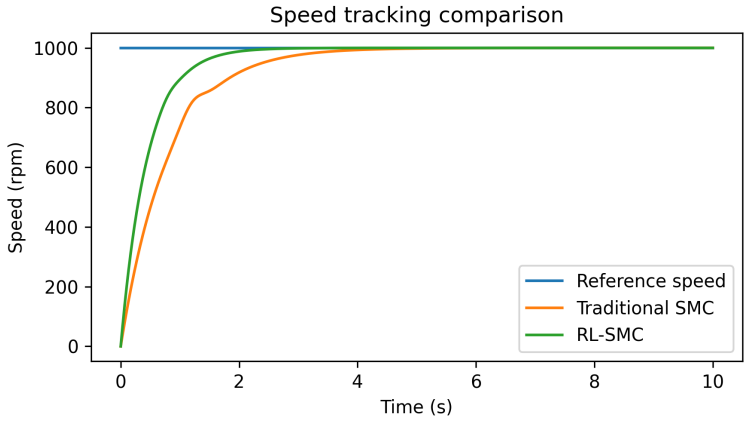

Fig. 10. Comparison of speed tracking for conventional SMC and RL-SMC

5 Conclusion

This study proposes a sensorless control method for permanent magnet synchronous motors, which combines a current-based sliding mode observer and a phase-locked loop (PLL). The observer reconstructs the rotor speed and angular position through electrical measurements, while the PLL improves signal extraction and suppresses high-frequency oscillations that are typically associated with discontinuous sliding mode laws. To validate the proposed method, a dual-closed-loop SVPWM drive system was built in MATLAB. Simulation results show that the improved observer using a saturation function can quickly track the rotor motion state and maintain a small estimation error under different operating conditions. Compared to traditional methods that rely on mechanical position sensors, the proposed method avoids additional sensing equipment and reduces adverse effects such as sensor failure, installation limitations, and environmental interference. In addition, it reduces hardware requirements and simplifies the drive system structure, which is particularly advantageous for wheeled mobile robots operating under conditions of vibration, shock, dust, or variable load. The observer exhibits satisfactory fault tolerance to motor parameter deviations, load abrupt changes, and external disturbances, demonstrating that reliable state reconstruction can still be achieved even when the operating model is not fully known. The estimated position and velocity signals provide stable feedback for vector control, thereby enabling precise electromagnetic torque regulation and smooth motor operation. Meanwhile, the combined use of saturation switching law and phase-locked loop filtering achieves a suitable balance between convergence speed, estimation

accuracy, and chattering suppression. Therefore, the entire system exhibits fast transient recovery, limited steady-state error, and robust dynamic characteristics. These findings demonstrate the feasibility of applying the proposed sensorless framework to an adaptive wheeled tracked robot driven by a permanent magnet synchronous motor. This method helps improve control reliability, environmental adaptability, and system integration, while reducing reliance on mechanical sensing elements. Future work will focus on prototype-based experiments to verify the algorithm's performance under real-world driving conditions and to study its performance under rapid acceleration, terrain changes, parameter drift, and complex load disturbances.

6 Acknowledgement

Research on Adaptive Sliding Mode Controller Control Parameter Optimization Based on Reinforcement Learning Algorithm and Simulation Analysis (Z26008).

References

[1] M.-M. Elkholy, M.-M. Algendy, E.-A. El-Hay, Modern control techniques and operational challenges in permanent magnet synchronous motors: a comprehensive review, Automation 6(4)(2025) 49.1-49.28. https://doi.org/10.3390/automation6040049

[2] I. Qureshi, V. Sharma, PMSM motor drive and their control schemes, Journal of Applied Research and Technology 22(2)(2024) 274-283. https://doi.org/10.22201/icat.24486736e.2024.22.2.2321

[3] A. Oztoprak, R. Hassanpour, A. Ozkan, K. Oztoprak, Security challenges, mitigation strategies, and future trends in wireless sensor networks: a review, ACM Computing Surveys 57(4)(2024) 1-29. https://doi.org/10.1145/3706583

[4] Y.-K. Song, Y.-Y. Tuo, J.-Y. Li, A neural adaptive prescribed performance controller for the chaotic PMSM stochastic system, Nonlinear Dynamics 111(16)(2023) 15055-15073. https://doi.org/10.1007/s11071-023-08634-0

[5] A. Beşkardeş, Y. Hameş, K. Kaya, A comprehensive review on fuzzy logic control systems for all, hybrid, and fuel cell electric vehicles, Soft Computing 28(13-14)(2024) 8183-8221. https://doi.org/10.1007/s00500-023-09454-5

[6] K. Shao, J.-C. Zheng, M.-Y. Fu, Review on the developments of sliding function and adaptive gain in sliding mode control, Journal of Automation and Intelligence 4(4)(2025) 266-272. https://doi.org/10.1016/j.jai.2025.06.001

[7] K. Li, J. Ding, X.-D. Sun, X. Tian, Overview of sliding mode control technology for permanent magnet synchronous motor system, IEEE Access 12(2024) 71685-71704. https://doi.org/10.1109/ACCESS.2024.3402983

[8] K. Shao, J.-C. Zheng, M.-Y. Fu, Review on the developments of sliding function and adaptive gain in sliding mode control, Journal of Automation and Intelligence 4(2025) 266-272. https://doi.org/10.1016/j.jai.2025.06.001

[9] Z. Chen, A. Dawara, X.-X, Zhang, H. Zhang, C.-Q. Liu, G.-Z. Luo, Adaptive sliding mode observer-based sensorless control for SPMSM employing a dual-PLL, IEEE Transactions on Transportation Electrification 8(2022) 1267-1277. https://doi.org/10.1109/TTE.2021.3112123

[10] Y. Liu, G.-F. Li, D. Jiang, J.-T. Yun, B. Tao, G.-Z. Jiang, J.-Y. Kong, B. Chen, Sliding mode controller by using adaptive exponential reaching law based on nonlinear disturbance observer, ISA Transactions 164(2025) 234-245. https://doi.org/10.1016/j.isatra.2025.05.028

[11] Y.-C. Zhong, K.-K. Zheng, S.-Q. Shen, Q.-Y. Xie, Z.-G. Xiao, Y.-T. Liu, An improved sliding mode control using disturbance observer for axial permanent magnet synchronous motor with dual-rotating rotors, Energies 18(2025) 2858.1-2858.17. https://doi.org/10.3390/en18112858

[12] H. Huang, S. Wang, C.-F. Yu, Z.-H. Sun, Y.-F. Zhang, K.-Q. Li, Fuzzy-adaptive super-twisting sliding mode observer for sensorless permanent magnet in-wheel motor control in electric vehicles, IEEE Transactions on Transportation Electrification 12(2026) 2207-2220. https://doi.org/10.1109/TTE.2025.3640616

[13] R.-G. Hart, E.-J. Griffis, O.-S. Patil, W.-E. Dixon, Lyapunov-based physics-informed long short-term memory (LSTM) neural network-based adaptive control, IEEE Control Systems Letters 8(2024) 13-18. https://doi.org/10.1109/LCSYS.2023.3347485

[14] L. Wang, C.-T. Freeman, E. Rogers, Disturbance observer-based predictive repetitive control with constraints, International Journal of Control 95(2022) 1060-1069.
https://doi.org/10.1080/00207179.2020.1839674
[15] L.-L. Gao, X. Liu, H. Liu, Analytical calculation of magnetic field and temperature field of surface mounted permanent magnet synchronous motor, Journal of Electrical Engineering & Technology 20(2025) 2249-2262.
https://doi.org/10.1007/s42835-024-02108-y
[16] Z. Wang, M.-R. Gu, M. Cheng, W. Hua, Modeling and predictive control of PMSM considering eddy-current reaction by vector magnetic circuit theory, IEEE Transactions on Industrial Electronics 71(2024) 8491-8502.
https://doi.org/10.1109/TIE.2023.3325569
[17] Q.-Q. Yuan, Y.-Y. Ma, Y.-Y. Huang, K. Xia, Y.-B. Yu, Adaptable sliding mode observer-based sensorless control with harmonic current compensation for dual three-phase PMSMs, Journal of Power Electronics 24(2024) 1889-1898.
https://doi.org/10.1007/s43236-024-00863-9
[18] K. Shao, J.-C. Zheng, M.-Y. Fu, Review on the developments of sliding function and adaptive gain in sliding mode control, Journal of Automation and Intelligence 4(4)(2025) 266-272.
https://doi.org/10.1016/j.jai.2025.06.001
[19] W.-J. Xu, S.-C. Qu, L. Zhao, H.-R. Zhang, An improved adaptive sliding mode observer for middle- and high-speed rotor tracking, IEEE Transactions on Power Electronics 36(1)(2021) 1043-1053.
https://doi.org/10.1109/TPEL.2020.3000785
[20] Q.-S. Yang, L.-L. Wang, Z.-Y. Qi, X.-H. Lu, Z.-J. Ma, F.-T. Yang, Analysis and optimization of high-frequency switching oscillation conducted CM current considering parasitic parameters based on a half-bridge power module, IEEE Transactions on Power Electronics 38(10)(2023) 12659-12674.
https://doi.org/10.1109/TPEL.2023.3291893
[21] R. Sreejith, B. Singh, Sensorless predictive current control of PMSM EV drive using DSOGI-FLL based sliding mode observer, IEEE Transactions on Industrial Electronics 68(7)(2021) 5537-5547.
https://doi.org/10.1109/TIE.2020.2996159
[22] R. Vijayapriya, P. Raja, M.-P. Selvan, Enhanced method of rotor speed and position estimation of permanent magnet synchronous machine based on stator SRF-PLL, Engineering Science and Technology, an International Journal 20(5)(2017) 1450-1459.
https://doi.org/10.1016/j.jestch.2017.09.004
[23] J. Zhang, Y.-L. Tang, F. Yu, Position sensorless control system of permanent magnet synchronous linear motor based on sliding mode observer with an improved phase-locked loop, Energy Engineering 118(4)(2021) 1083-1094.
https://doi.org/10.32604/EE.2021.014482
[24] Z. Zhao, R. Leidhold, On the estimation error of position sensorless control of PM synchronous motors, Energy Reports 8(Suppl 1)(2022) 1059-1065.
https://doi.org/10.1016/j.egyr.2021.11.177
[25] W. Wang, Y. Hong, Model predictive current control method of dual three-phase permanent magnet synchronous motor based on improved SVPWM, Electrical Engineering 107(4)(2025) 4517-4525.
https://doi.org/10.1007/s00202-024-02773-2
[26] Q. Abdullah, N. Farah, M.-S. Ahmed, N.-S.-M. Shah, Ö. Aydoğdu, M.-H.-N. Talib, Sensorless speed control of induction motor drives using reinforcement learning and self-tuning simplified fuzzy logic controller, IEEE Access 12(2024) 136485-136501.
https://doi.org/10.1109/ACCESS.2024.3435529
[27] D.-M. Stojić, T.-B. Šekara, Multi-resonant current controller for grid-tied inverters with LCL filters based on pole placement under robustness constraints, Journal of Power Electronics 25(10)(2025) 1942-1953.
https://doi.org/10.1007/s43236-025-01016-2
[28] W.-J. Xu, S.-C. Qu, J.-H. Zhao, H.-R. Zhang, X.-N. Du, An improved full-order sliding-mode observer for rotor position and speed estimation of SPMSM, IEEE Access 9(2021) 15099-15109.
https://doi.org/10.1109/ACCESS.2021.3052085
[29] J. Chen, Q.-M. Luo, Y.-Q. Wei, X.-Y. Zhang, X. Du, The sustained oscillation modeling and its quantitative suppression methodology for GaN devices, IEEE Transactions on Power Electronics 36(7)(2021) 7927-7941.
https://doi.org/10.1109/TPEL.2020.3043472
[30] J.-Q. Deng, L.-Y. Zhang, W.-C. Xue, Q.-L. Bao, Y. Mao, Active compression on unknown disturbance and uncertainty via extended state observer, IEEE/CAA Journal of Automatica Sinica 12(9)(2025) 1878-1892.
https://doi.org/10.1109/JAS.2025.125342
[31] Y.-X. Yang, W.-S. Robertson, A. Jafari, M. Arjomandi, Optimising coil design based on sensitivity analysis of magnetic force induced between misaligned coil pairs, Electrical Engineering 107(12)(2025) 15317-15328.
https://doi.org/10.1007/s00202-025-03327-w